Cortical Plasticity is associated with Blood-Brain-Barrier Modulation

Evyatar Swissa[1], Uri Monsonego[2], Lynn T. Yang[3,4], Lior Schori[2], Lyna Kamintsky[5], Sheida Mirloo[5], Itamar Burger[2], Sarit Uzzan[6], Rishi Patel[3], Peter H Sudmant[3], Ofer Prager[1,2], Daniela Kaufer[3,4] and Alon Friedman[1,2,5*]

[1] Department of Brain and Cognitive Sciences, The School of Brain Sciences and Cognition, Zlotowski Center for Neuroscience, Ben-Gurion University of the Negev, Beer-Sheva, Israel

[2] Department of Physiology and Cell Biology, Faculty of Health Sciences, Ben-Gurion University of the Negev, Beer-Sheva, Israel

[3] Department of Integrative Biology, University of California, Berkeley, CA 94720, USA

[4] Helen Wills Neuroscience Institute, University of California, Berkeley, CA 94720, USA

[5] Department of Medical Neuroscience, Dalhousie University, Halifax, Nova Scotia, Canada

[6] Department of Clinical Biochemistry and Pharmacology, Faculty of Health Sciences, Ben-Gurion University of the Negev, Beer-Sheva, Israel

Correspondence to: **Prof. Alon Friedman**, Ben-Gurion University of the Negev, P.O.B. 653 Beer-Sheva, 8410501 Israel, Email: alonf@bgu.ac.il

Summary

Brain microvessels possess the unique properties of a blood-brain barrier (BBB), tightly regulating the passage of molecules from the blood to the brain neuropil and vice versa. In models of brain injury, BBB dysfunction and the associated leakage of serum albumin to the neuropil have been shown to induce pathological plasticity, neuronal hyper-excitability, and seizures. The effect of neuronal activity on BBB function and whether it plays a role in plasticity in the healthy brain remain unclear. Here we show that neuronal activity induces modulation of microvascular permeability in the healthy brain and that it has a role in local network reorganization. Combining simultaneous electrophysiological recording and vascular imaging with transcriptomic analysis in rats, and functional and

BBB-mapping MRI in human subjects we show that prolonged stimulation of the limb induces a focal increase in BBB permeability in the corresponding somatosensory cortex that is associated with long-term synaptic plasticity. We further show that the increased microvascular permeability depends on neuronal activity and involves caveolae-mediated transcytosis and transforming growth factor beta signaling. Our results reveal a role of BBB modulation in cortical plasticity in the healthy brain, highlighting the importance of neurovascular interactions for sensory experience and learning.

Keywords: Blood-brain barrier, synaptic plasticity, magnetic resonance imaging, caveolae-mediated transcytosis, transforming growth factor beta.

Introduction

The intricate components comprising the blood-brain barrier (BBB) regulate the bi-directional transport of molecules between the brain and the circulatory system, keeping tight control over the brain's extracellular environment, thus permitting the normal function of the neurovascular unit (NVU) (Chow and Gu, 2015). A leaky dysfunctional BBB is common in most neurological disorders and is associated with the extravasation of serum proteins into the neuropil. The extravasation of serum albumin into the neuropil activates transforming growth factor β (TGF-β) signaling in astrocytes, leading to reduced buffering of extracellular potassium and glutamate, changes in the extracellular matrix, excitatory synaptogenesis, and cortical network re-wiring, together increasing neuronal excitability and lowering seizure threshold (David et al., 2009; Heinemann et al., 2012; Ivens et al., 2007; Weissberg et al., 2015). An increase in BBB permeability following brain insults has been shown to partly depend on

neuronal excess release of glutamate due to hypoxia (Revah et al., 2016), seizures, or spreading depolarizations (Vazana et al., 2016). Whether excess neuronal activity in the healthy brain modulates microvascular permeability is not known. Whisker stimulation (1 hour, 2 Hz) in rats increases the transport of insulin-like growth factor-I, likely via specific receptor-mediated transcytosis (RMT) (Nishijima et al., 2010). RMT was also shown to underlie transport of plasma proteins into the brain of young healthy mice (Yang et al., 2020). A circadian modulation of BBB permeability has been recently shown in Drosophila (Zhang et al., 2018) and mice (Pulido et al., 2020), suggesting a role for BBB modulation in healthy brain functions (Pan and Kastin, 2017). However, the mechanisms and role of changes in BBB properties in the healthy brain are not known.

Results

Stimulation increases BBB permeability

To test for changes in BBB permeability in response to stimulation we combined electrophysiological recordings with BBB imaging using intravital microscopy (Figure 1, see timeline of stimuli in Figure 1a). First, we localized vascular response to sensory stimulation by wide-field imaging of arterial diameter and monitoring change in total hemoglobin (HbT) signal during a 1 min stimulation of the limb (Figure 1b-d) (Bouchard et al., 2009). Fluorescent angiography before and immediately after 30 min of limb stimulation showed local extravasation of the tracer sodium fluorescein (NaFlu) around the responding blood vessels, indicative of BBB leakage (Figure 1f-g). Histological analysis confirmed the presence of NaFlu in the extravascular space around small vessels in the somatosensory cortex, contralateral (and not ipsilateral) to the stimulated limb (Figure 1m-n). Next, we intravenously injected a separate cohort of

rats with either the albumin-binding dye Evans blue (EB) or albumin conjugated with Alexa Fluor 488 (Alexa488-Alb) without performing craniotomy. Brain extravasation of both dyes was found in the contralateral hemisphere, indicating the presence of serum albumin in the neuropil (Figure 1h-k). ELISA performed in cortical tissue at different time points after stimulation confirmed a higher concentration of albumin in the stimulated sensorimotor cortex early after stimulation (30 min) compared to non-stimulated sham-controls, that declined 4- and 24-hours post-stimulation (Figure 1l). As a positive control, brain tissues were also prepared from rats subjected to photothrombosis (PT)-induced ischemia. Albumin concentrations in the peri-ischemic cortex 24 hours following PT were significantly higher compared to sham and all time-points after stimulation (Figure S1d). These results suggest that the focal modulation of BBB permeability following stimulation is distinct from the extensive BBB dysfunction observed in injury models.

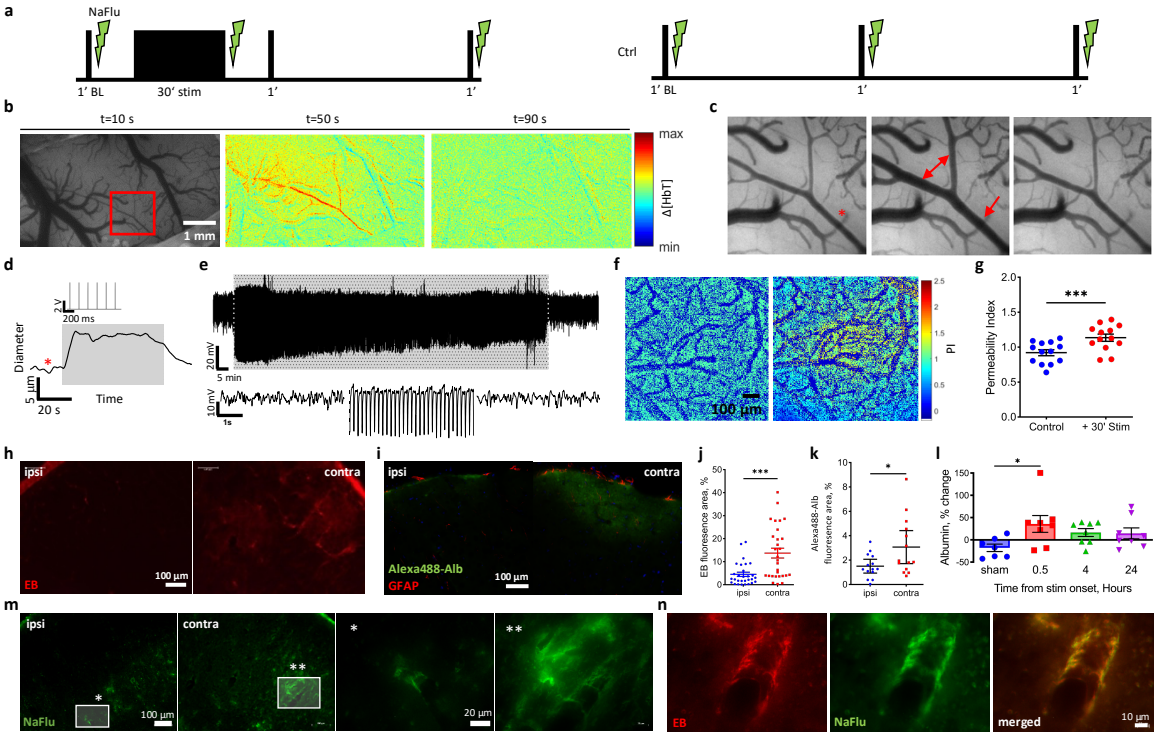

Figure 1: Limb stimulation modulates blood-brain barrier permeability. a. Timelines of the experimental protocols for stimulations and imaging with 30 min stimulation (left) and without (right). **b.** Image of the cortical window over the rat sensorimotor cortex, followed by maps of the change in HbT concentration showing the evolution of the hemodynamic response during and after stimulation. Red rectangle marks the responding region magnified in c. **c.** Images of the responding arteriole in the rats' cortex before (left) during (middle) and after stimulation (right). Red arrows mark the responding arteriole. **d.** The responding arterioles' diameter during 1 min stimulation. Gray area corresponds to time of stimulation **e.** Top: local field potential (LFP) trace from the corresponding region in L2/3 sensorimotor cortex before during (greyed area) and after 30 min limb stimulation. Bottom: 5 s excerpts of the above trace (left-to-right: before during and after stimulation). **f.** NaFlu permeability maps before (left) and after 30 min stimulation (right) showing tracer accumulation around a responding arteriole. **g.** Permeability index is higher after stimulation compared to baseline. Wilcoxon, n=13 rats, mean ± SEM. **h-i.** Fluorescence images of cortical sections of stimulated rats injected with the albumin-binding dye Evans blue (h) and Alexa-488-Alb (i). **j-k.** Total fluorescence of EB (j) and Alexa488-Alb (k) after stimulation in the contralateral hemisphere compared to the ipsilateral hemisphere. Wilcoxon, EB (n=5 rats, 30 sections), Alexa488-Alb (n=5 rats, 15 sections), mean ± SEM. **l.** Albumin concentration in the contralateral hemisphere relative to the ipsilateral in different timepoints after stimulation, compared to sham stimulation. Kruskal-Wallis with FDR correction, 0.5 and 4 h post-stimulation n=8, sham n=7, mean ± SEM. **m.** Cortical sections of the area of limb representation from both hemispheres of a stimulated rat (left), and higher magnification images (right) **n.** Fluorescence image of a cortical small vessel in the stimulated hemisphere showing extravascular accumulation of EB and NaFlu. *$p<0.05$, ***$p<0.001$.

BBB permeability is associated with synaptic potentiation

To study changes in brain activity during repetitive stimulation of the limb, we measured somatosensory evoked potentials (SEP) by averaging neuronal response to a 1 min test stimulation before and after the 30 min stimulation train (6 Hz, 2 mA). SEP amplitudes and area under the curve were increased in stimulated, but not in control, cortices (Figure 2a-e). Potentiation lasted for >5 h (until the end of each experiment) and was therefore indicative of long-term potentiation (LTP).

To test whether stimulation-induced albumin extravasation has a role in LTP, we recorded local field potentials (LFP) before and after exposure of the cortex to 0.1 mM albumin (corresponding to 25% of serum concentration) (Ivens et al., 2007). Albumin application increased the amplitude and frequency of spontaneous activity (Figure 2f). Neuronal response to the stimulation showed synaptic potentiation in the presence of albumin compared to that recorded under aCSF (Figure 2g-i), indicating that cortical exposure to serum albumin results in synaptic potentiation.

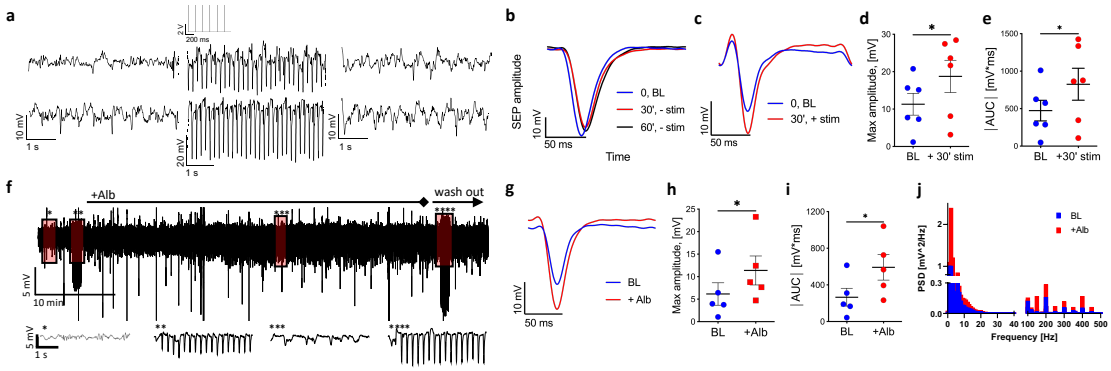

Figure 2: Stimulation and cortical perfusion of serum albumin induce LTP. a. Top: LFP trace from the rat L2/3 sensorimotor cortex before (left) during (middle) and after (right) 1 min test stimulation (6 Hz, 2 mA). Bottom: LFP trace from the same rat during 1 min test stimulation, following a 30 min stimulation. **b.** The somatosensory evoked potential (SEP) of 1 min test stimulation at baseline (BL) and after 30 and 60 minutes (blue, red, black, respectively, each averaged over 360 stimuli). **c.** SEP in response to 1 min test stimulation at baseline (blue) and following a 30 min stimulation (red). **d.** Maximum amplitude of the SEP (absolute values) following a 30 min stimulation compared to baseline (n=6). **e.** Area under curve (AUC) of the SEP following a 30 min stimulation compared to baseline. **f.** Top: 1 hour LFP trace from a representative rat. Bottom: 5 s magnifications of the above trace at selected time points (noted by asterisks). Left to right: baseline activity; during 1 min test stimulation; following cortical application of 0.1 mM albumin (Alb); during 1 min test stimulation post-Alb. **g.** SEP amplitude during 1 min stimulation at baseline (normal aCSF, blue) and following 0.1 mM Alb (red). **h.** Maximum amplitude of the SEP during 1 min stimulation post-Alb compared to baseline (n=5). **i.** AUC of the SEP post-Alb compared to baseline. **j.** Power spectrum density of 10 min spontaneous activity before (blue) and post-Alb (red). *p<0.05, Wilcoxon, data are mean ± SEM.

BBB modulation is activity-dependent

To test the neurotransmission pathways involved in regulation of BBB permeability during stimulation we exposed the cortical window to selective antagonists of ionotropic glutamate receptors (Figure 3a). The AMPA/kainate receptor blocker CNQX prevented the stimulation-induced BBB modulation, whereas the NMDAR blocker AP5 did not (Figure 3b-c). CNQX also reversibly blocked synaptic activity and prevented the vascular response to neuronal activation, indicated by the absence of vasodilation (AKA "neurovascular coupling"; Figure 3d-e, Figure S2b, S3a). These results indicate that stimulation-induced BBB modulation was mediated by neuronal activation. In contrast, AP5 did not affect baseline SEP (Figure 3d-e), nor the vascular response (Figure S2b, S3b). Synaptic potentiation was blocked under both CNQX or AP5 (Figure 3e-f, Figure S2a), consistent with the crucial role of AMPA and NMDA

receptors in synaptic plasticity. Next, we tested for molecular correlates of synaptic strength by comparing postsynaptic density 95 (PSD-95) expression levels in the cortex at different time points. PSD-95 is known to increase following LTP and AMPAR trafficking (El-Husseini et al., 2000; Holtmaat and Svoboda, 2009). Western blot analysis showed significantly higher levels of PSD-95 expression in stimulated rats as compared to sham, at both 30 min and 24 h after stimulation (Figure S2c-d).

Albumin extravasation and LTP require caveolae-mediated transcytosis

In endothelial cells, albumin is transported mainly via caveolae-mediated transcytosis (CMT) through binding to the gp60 receptor (Tiruppathi et al., 1997). To test whether CMT mediates stimulation-induced transcytosis of albumin(John et al., 2003) we perfused the exposed cortex with mβCD, which inhibits albumin uptake by disrupting caveolae (Schnitzer and Oh, 1994; Skotland et al., 2020). Cortical application of mβCD prevented stimulus-induced BBB opening (Figure 3i), without affecting vascular response to stimulation (Figure S3d). mβCD also prevented stimulus-induced LTP (Figure 3j, l), further supporting the role of CMT-mediated albumin extravasation in activity-dependent plasticity in vivo.

BBB modulation and LTP involve TGF-β signaling

Under pathological conditions, synaptogenesis and pathological plasticity that follow BBB dysfunction are mediated by the activation of TGF-βR1 signaling in astrocytes (Weissberg et al., 2015). TGF-β1 was also shown to directly induce BBB opening in endothelial cell cultures (McMillin et al., 2015), and to regulate hippocampal synaptic plasticity (Dahlmanns et al., 2022; Gradari et al., 2021). We therefore tested the effect of stimulation in the presence of the specific TGF-βR1 blocker SJN2511 (SJN, 0.3

mM)[7]. Cortical exposure to SJN prevented stimulation-induced BBB opening (Figure 3g-h) with no effect on neurovascular coupling (Figure S3e). SJN also prevented stimulation-induced LTP (Figure 3j-k). These results demonstrate that TGF-β signaling is required for activity-dependent BBB modulation, and the consequent activity-dependent plasticity, but not for the neurovascular coupling.

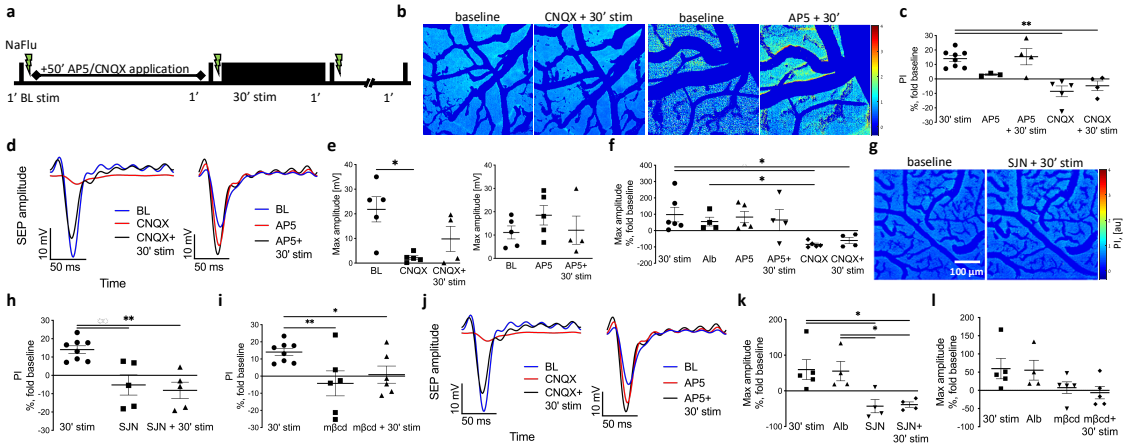

Figure 3: Stimulation-induced plasticity is associated with BBB modulation. a. Timeline of the experimental protocol for stimulations and imaging with blockers application. **b.** NaFlu permeability maps of the cortical window before (control, left), and after CNQX/AP5 + 30 min stimulation (stim, right). **c.** PI following CNQX and AP5 compared to a 30 min stimulation, presented as % change from baseline (30 min stim n=6, AP5 n=4, CNQX n=5). **d.** SEP amplitude in response to 1 min test stimulation. baseline (blue); following cortical application of CNQX (left, red) or AP5 (right, red); following CNQX + 30 min stimulation (left, black); and following AP5 + 30 min stimulation (right, black); **e.** Left: Max SEP amplitude to 1 min test stimulation following CNQX compared to baseline. Right: SEP amplitude following AP5 compared to baseline. **f.** SEP amplitude following 30 min stimulation or albumin application compared to AP5, AP5 + 30 min stimulation, CNQX and CNQX + 30 min stimulation. (% change from baseline). **g.** Permeability maps before (control, left), and after SJN + 30 min stimulation (right). **h.** PI following SJN application compared to 30 min stimulation (n=5). **i.** PI following mβCD compared to a 30 min stimulation (n=6). **j.** SEP amplitude: baseline (blue); following SJN (black); following SJN + 30 min stimulation (red); and following mβCD (right). **k-l.** SEP amplitude following 30 min stimulation or albumin application compared to SJN and SJN + 30 min stimulation (k), and mβCD, mβCD + 30 min stimulation (l). *p<0.05, **p<0.001, Kruskal-Wallis with FDR correction; data are mean ± SEM. (c-f, h-l).

Regulation of BBB transport and plasticity genes

To explore gene-expression changes related to our stimulation protocol, we conducted bulk RNA-sequencing transcriptome analysis of tissue dissected from the sensorimotor area of the cortex contralateral and ipsilateral to stimulated limb. Tissue harvested 1 and 24 h post-stimulation showed differentially expressed genes (DEGs) in the contralateral ("stimulated") compared to the ipsilateral ("non-stimulated") cortex

(13.2% and 7.3% 24 and 1 h, respectively Figure 4a). To assess the variability between paired samples of stimulated and non-stimulated cortex of each animal at two time points following stimulation (24 h vs 1 h) we used the Jensen–Shannon divergence metric (JSD). JSD calculations using normalized counts indicated that the RNA expression 24 h after stimulation was significantly different from that of rats 1 h after stimulation (Figure S4b). Gene Ontology (GO) pathway enrichment analysis of DEGs from stimulated rats indicated DEGs were primarily involved in synaptic plasticity processes (Figure 4b). A larger number of synaptic plasticity related DEGs was found in the contralateral cortex of stimulated rats compared to ipsilateral (Figure 4d). BBB structure, integrity, and tight junction related genes were largely unaffected by stimulation (Figure 4d). In contrast, a larger amount of BBB transporter genes such as solute carrier transporters (Slc) and ATP-binding cassette (ABCs) families were differentially expressed in the stimulated compared to the non-stimulated cortex (Figure S4d-e). Additionally, DEGs and enrichment analyses were consistent with activation of TGF-β signaling pathway (Figure 4e). Transcriptome analysis did not indicate a general brain inflammatory response, suggesting that the stimulation protocol is not associated with the transcriptional change observed in BBB dysfunction under pathological conditions (Cacheaux et al., 2009; Kim et al., 2017) (Figure 4e). Analysis of vascular cell-specific DEGs (Vanlandewijck et al., 2018) showed significantly more arterial smooth muscle cells specific genes in the stimulated cortex (Figure 4c, Figure S4c). These results support the roles of stimulation-induced modulation of BBB transcellular transport and TGF-β signaling in activity-dependent plasticity (Figure S5).

Physiological BBB modulation in the human brain

Finally, we tested for neuronal activity-induced BBB modulation in healthy human volunteers by measuring the blood-oxygenation-level dependent (BOLD) response to a 30 min stress-ball squeeze task and blood-to-brain transport using dynamic contrast-enhanced (DCE) MRI (Figure 5a-b). As expected, BOLD response was found in the pre- and post- central gyrus, corresponding with the primary motor and sensory cortices, respectively, of the hemisphere contralateral to the squeezing hand (Figure 5c-d). DCE-MRI showed higher BBB permeability to Gd-DOTA in sensory/motor-related areas of subjects performing the task, as compared to controls (Figure 5e-g). Comparison of the spatial distribution of functional and permeability changes revealed a higher percentage of activated regions with modulated BBB in task performers than in control subjects (Figure 5e-g).

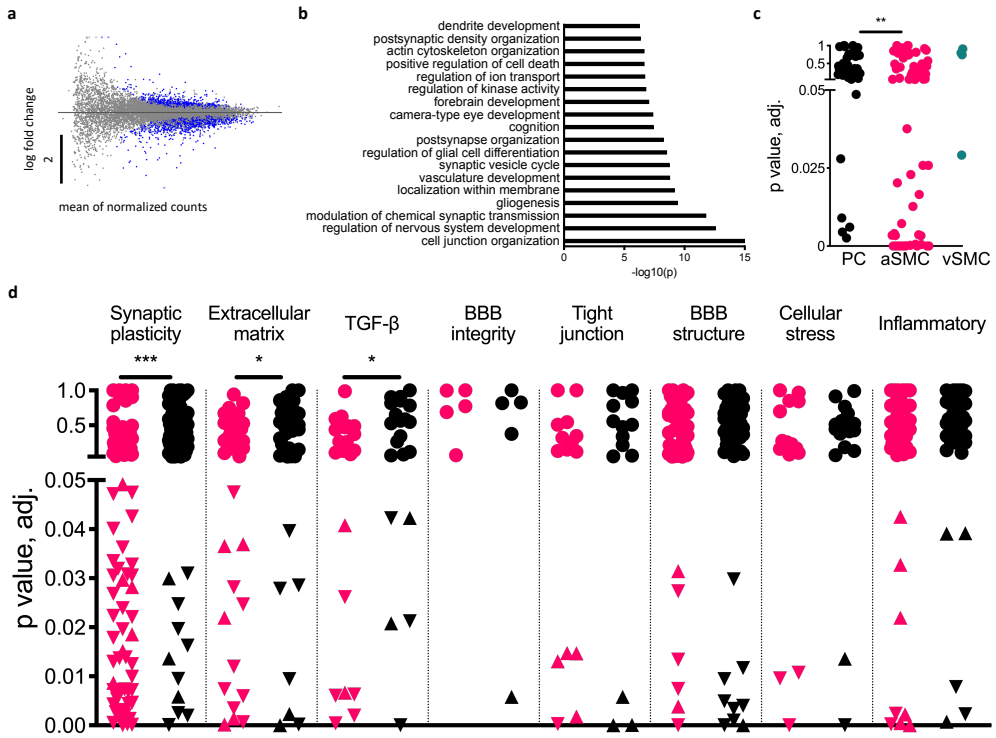

Figure 4: Neuronal activity regulates BBB transport and synaptic plasticity genes. a. Scatter plot of gene expression from RNA-seq in the contralateral cortex 24 vs. 1 h after stimulation. The x axis represents the log fold change and the y axis represents the mean expression levels. Blue dots indicate statistically significant differentially expressed genes (DEGs) by Wald Test (n=8 rats per group). **b.** Top Gene Ontologies (GO) enriched terms in the contralateral cortices of rats 24 vs. 1 h after stimulation. **c.** Vascular cell specific DEGs to pericytes (PC), arterial smooth muscle cells (aSMC), and venous smooth muscle cells (vSMC). **d.** Scatter plot of DEGs divided by groups of interest: BBB properties, NVU properties, Synaptic plasticity, and inflammatory related genes in the contralateral

(red) vs. ipsilateral (black) cortices of stimulated rats. Upward and downward triangles indicate up- and down-regulated genes respectively.

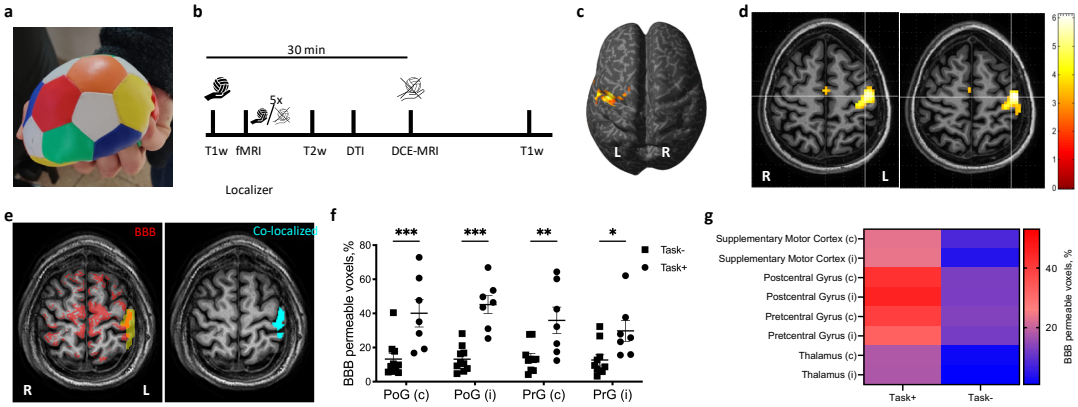

Figure 5: Cortical activation in fMRI co-localizes with BBB modulation. a. Subjects were given an elastic stress-ball to squeeze continuously for the length of the session (30 min). **b.** Timeline of the experimental protocol for task performance and MRI sequences. **c.** Activation map for the localizer task displayed over the inflated brain of an exemplary subject. ($p<0.05$, FWE corrected, neurologic convention). **d.** Activation maps for the localizer task displayed over anatomical axial slices of an exemplary subject. ($p<0.05$, FWE corrected, radiologic convention). **e.** Left: Superimposed masks of BBB modulated voxels (red) and fMRI activation (yellow). Right: Co-localized voxels map on the same slice (cyan). **f.** BBB modulation in M1 (precentral gyrus, PrG) and S1 (postcentral gyrus, PoG) for subjects performing the task compared to controls (% area). **g.** Heatmap of BBB modulated voxels percentage in motor/sensory related areas of task vs. controls. *$p<0.05$, ***$p<0.001$, two-way ANOVA with FDR correction, task n=6, controls n=10, (i–ipsi, c-contra). All data are mean ± SEM.

Discussion

In this study, we tested whether neuronal activity modulates BBB permeability under physiological conditions. We showed that physiological stimulation of the paw modulates BBB permeability and results in increased extravasation of both low- and high- molecular weight tracers. The increase in BBB permeability due to neuronal activation is focal, localized to the cortical area corresponding to the stimulation. These findings are in agreement with recent studies demonstrating circadian- or age-dependent changes in transport of proteins and growth factors through the BBB (Pulido et al., 2020; Yang et al., 2020) or in response to whisker stimulation (Nishijima et al., 2010). Our results directly show that prolonged sensory-motor activation is associated with blood-to-brain transport of serum albumin. Notably, the spatial distribution and

extent of extravasation in response to physiological stimulation is significantly lower than that observed under pathological conditions (Figure S1d and (Prager et al., 2010; Schoknecht et al., 2014)).

The involvement of CMT in the mechanism underlying the stimulation-induced transport of albumin across the BBB is in line with the emerging evidence for a physiological role for CMT in BBB functions including neurovascular coupling (Andreone et al., 2017; Chow et al., 2020). This is consistent with our in vivo imaging results showing increased caveolae-mediated permeability in arterioles. However, in our experiments CMT inhibition did not impair arteriolar dilation to limb stimulation, likely due to the involvement of other pathways such as endothelial nitric oxide synthase.

Previous studies from our group showed that under models of brain injury, extravasated albumin binds to TGF-βR in astrocytes, resulting in TGF-β signaling and associated pathological plasticity are prevented by TGF-βR blockers following albumin exposure in brain slices (Ivens et al., 2007), and in vivo (Weissberg et al., 2015). We demonstrated here that stimulation-induced BBB opening is prevented by blocking TGF-βR. Additionally, Blocking CMT or TGF-βR prevented the potentiation, without affecting baseline synaptic transmission, SEP properties, or the physiological hemodynamic response. Interestingly, our results are reinforced by a recent work showing astrocyte-derived extracellular vesicles enhance spine and synapses formation in vitro via TGF-β signaling in neurons (Patel and Weaver, 2021). Moreover, the TGF-β signaling pathway was recently shown to play a role in environmental enrichment-induced synaptic plasticity (Dahlmanns et al., 2022) as well adult neuroplasticity in the

hippocampus (Gradari et al., 2021). Taken together, these results suggest that stimulation-induced BBB modulation may play a role in synaptic potentiation, indicating a mechanistic link between vascular and neuronal modulations.

The low-MW tracer NaFlu does not cross the BBB under normal conditions (Saunders et al., 2015). Previous studies suggested that transport of NaFlu across the BBB is mediated by the solute-carrier transporter organic anion transporter-3 (OAT3/SLC22A8) and the efflux transporters multidrug resistance proteins (MRP1,2/ABCC1,2) (Hawkins et al., 2007). Our RNA-seq analysis showed significant upregulation of OAT3 in the stimulated cortex, but not in the unstimulated cortex. No differences in MRP genes expression were observed.

Animal studies have linked physical exercise to neural and vascular plasticity, showing growth factor-dependent cell proliferation associated with the growth of new neurons (neurogenesis) and new vasculature (angiogenesis) (Hillman et al., 2008; Kleim et al., 2002). Plasticity of both sensory and motor systems in humans is observed following sensorimotor adaptation to motor tasks such as juggling (Draganski et al., 2004), playing a video game (Sagi et al., 2012) or even simple motor training such as repetitive finger movements (Classen et al., 1998). A simple motor task such as squeezing an elastic stress-ball continuously does not require visuomotor skill and does not involve other modalities or guided instructions, which might modulate brain activity (Halder et al., 2005). Such a task entails neuronal activity localized to the motor and sensory areas without high-level processing or cross-modality processes to induce use-dependent plasticity. Our results demonstrate, for the first time, that repetitive sensorimotor

activation within a physiological range is associated with increased BBB permeability in the human cerebral cortex.

The magnitude and duration of neuronal activity required for modulation of BBB permeability and how they are balanced to avoid pathology remain to be explored in future studies. Our findings indicate a role for physiological modulation of BBB permeability in synaptic strength and plasticity (Figure S5). These findings stress the importance and challenges of studying neurovascular interactions in humans and their implications on health and disease.

Acknowledgments

This study was supported by the Israel Science Foundation (Awards No. 717/15 and 2254/20), Canadian Institutes of Health Research (CIHR Award No. PJT 148896), and the European Research Area Network Neuron Award (Award No. NDD 168164). We thank QB3 Genomics Sequencing Laboratory, UC Berkeley, Berkeley, CA, RRID:SCR_022170 for using their facilities.

Author Contributions

E.S., A.F., and O.P. conceived and designed the project; E.S., U.M., O.P., L.T.Y., L.S., S.U., and I.B. performed experiments; E.S, L.K., and S.M performed magnetic resonance imaging analysis; L.T.Y. performed bioinformatic experiments; L.T.Y., P.S., R.P., and E.S. analyzed the bioinformatic data; E.S. and A.F. wrote the manuscript with substantial input from D.K. and O.P. All authors reviewed the manuscript.

Declaration of Interest

The authors declare no competing interests.

Methods

Resource availability

Lead contact

Further information and requests for data or code should be directed to and will be fulfilled by the lead contact, Alon Friedman (alonf@bgu.ac.il).

Materials availability

This study did not generate new unique reagents.

Experimental model and subject details

All experimental procedures were approved by the Animal Care and Use Ethical Committee at the Ben-Gurion University of the Negev, Beer-Sheva, Israel.

Experiments were performed on adult Sprague Dawley male rats (300-350 g; Harlan Laboratories).

Method details

Animal preparation and surgical procedures

Adult Sprague Dawley male rats (300-350 g; Harlan Laboratories) were kept under a 12:12 h light and dark regimen and supplied with drinking water and food ad libitum. Surgical procedures were performed as reported previously(Prager et al., 2010). Rats were deeply anesthetized by intraperitoneal administration of ketamine (100 mg/ml, 0.08 ml/100 g) and xylazine (20 mg/ml, 0.06 ml/100 g). The tail vein was cannulated, and animals were placed in a stereotactic frame under a SteREO Lumar V12

fluorescence microscope (Zeiss). Body temperature was continuously monitored and kept stable at 37 ± 0.5°C using a feedback-controlled heating pad (Physitemp). Heart rate, breath rate, and oxygen saturation levels were continuously monitored using MouseOx (STARR Life Sciences). A cranial section (4 mm caudal, 2 mm frontal, 5 mm lateral to bregma) was removed over the right sensorimotor cortex. The dura and arachnoid layers were removed, and the exposed cortex was continuously perfused with artificial CSF (aCSF (Prager et al., 2010), containing (in mM): 124 NaCl, 26 $NaHCO_3$, 1.25 NaH_2PO_4, 2 $MgSO_4$, 2 $CaCl_2$, 3 KCl, and 10 glucose, pH 7.4). In some experiments the following blockers were used: D-(-)-2-Amino-5-phosphonopentanoic acid (AP5, 50 μM), 6-cyano-7-nitroquinoxaline-2,3-dione (CNQX, 50 μM), methyl-β-cyclodextrin (MβCD, 10 μM), or SJN2511 (SJN, 0.3 mM (Weissberg et al., 2015)) were added to the aCSF. To simulate BBB opening, bovine serum albumin (Alb, 0.1 mM (Seiffert et al., 2004)) was added to the aCSF.

In-vivo imaging

Dynamic imaging of regional cerebral blood flow, optical imaging of cortical oxygenation, neurovascular coupling (NVC), and vessel diameter measurements were carried out as previously described (Bouchard et al., 2009; Levi et al., 2012; Prager et al., 2010). Before, during, and after electrical limb stimulation, full-resolution (2560 x 2160 px) images were obtained for regional localization of the hemodynamic response, followed by acquisition of localized (512 × 512 px) images of cortical surface vessels (2 frames/s, EMCCD camera, Neo DC-152Q-COO-FI; Andor Technology) under 525/50 band pass filter (38 HE, Zeiss). Images were analyzed offline using in-house MATLAB (MathWorks) scripts.

Fluorescent angiography and BBB permeability measurements and analyses were performed as described previously (Prager et al., 2010; Vazana et al., 2016). The non-

BBB permeable fluorescent dye sodium fluorescein (NaFlu) was injected intravenously (0.2 ml, 1 mg/ml). Images of cortical surface vessels were obtained (5 frames/s, 512 × 512 pixel) before, during, and after injection of the tracer. Images were analyzed offline using MATLAB as described (Vazana et al., 2016). Briefly, image registration and segmentation were performed to produce a binary image, separating blood vessels from extravascular regions. Signal intensity changes over time and space were then analyzed so that each pixel was represented by intensity versus time (IT) curve. An arterial IT curve [arterial input function (AIF)] was created by spatially averaging signal intensity through time in the responding artery. A BBB permeability index (PI) was calculated for each extravascular pixel as the ratio between IT curve and AIF. The PI indicates how much tracer remains in extravascular tissue in relation to the applied amount. PI > 1 indicates tracer accumulation was therefore defined a permeable BBB.

Electrophysiology

Stimulation protocol

The left forelimb or hind limb of the rat was stimulated using Isolated Stimulator device (AD Instruments) attached with two subdermal needle electrodes (0.1 ms square pulses, 2-3 mA) at 6 Hz frequency. Stimulus-evoked potentials were recorded in the somatosensory cortex. Short-duration stimulation consisted of 360 pulses (60 s) and delivered before (as baseline) and after long-duration stimulation (30 min). In control and albumin rats only short-duration stimulations were performed.

In-vivo recordings

Local field- and somatosensory evoked potentials (LFP, SEP) were recorded using a glass microelectrode (1.5 x 1.1 mm, 1-2 µm tip, 2-10 MΩ) filled with aCSF, which was inserted with an isolated, chlorinated silver wire connected to a headstage and amplifier

(EXT-02B, npi electronic, Germany). The electrode was attached to a digital micromanipulator (MP-225, Sutter Instruments, CA, USA) and was carefully placed over the identified area of the sensorimotor response to the stimulation.

Data acquisition and analyses

Data acquisition was performed using PowerLab and LabChart (AD Instruments), for stimulation, and extracellular recordings. Signals were digitized (1 kHz) and filtered (high-pass 1 Hz, low pass 45 or 300 Hz). Analyses were performed using in house MATLAB scripts. To measure synaptic plasticity, the peak-to-peak amplitude between the initial largest positive and negative peaks occurring during the 10–160 ms post-stimulus period, as well as the absolute area under curve (AUC) of the SEP waveform were used for statistical analysis.

Histology and immunohistochemistry

To assess BBB permeability, separate cohorts of rats were anesthetized and stimulated without craniotomy surgery and either Evan's blue (EB, 2%, 20 mg/ml, n=5), or Alexa-Fluor 488-labeled bovine serum albumin (Alexa488-Alb, 1.7 mg/ml, n=5) were injected to the tail vein. Rats were then transcardially perfused with cold phosphate-buffered saline (PBS) followed by PBS containing 4% paraformaldehyde (PFA). Brains were then removed, fixed overnight (4% PFA, 4°C), cryoprotected with sucrose gradient (10% followed by 20 and 30% sucrose in PBS) and frozen in optimal cutting temperature (OCT) compound. Coronal sections (40-µm thick) were obtained using a freezing microtome (Leica Biosystems) and imaged for dyes extravasation using a fluorescence microscope (Axioskop 2; Zeiss) equipped with a CCD digital camera (AxioCam MRc 5; Zeiss).

For immunostaining, brain slices were incubated in blocking solution (5% donkey serum in 0.1% Triton X-100/tris-buffered saline (TBS)), then incubated in primary antibody, followed by secondary antibody. Finally, slices were mounted and stained for DAPI (DAPI-Fluoromount-G, Invitrogen) to label nuclei. Staining was performed against glial fibrillary acidic protein (mouse anti GFAP−Cy3™, Sigma-Aldrich, C9205), Secondary antibody was anti-mouse Alexa Fluor 488 (Thermo-Fisher, A21206).

Immunoassays

Enzyme-linked immunosorbent assay (ELISA) for albumin extravasation

To assess the degree of albumin extravasation following stimulation, forty adult Sprague Dawley male rats (200-300g) were randomly divided into five groups. Rats were anesthetized (ketamine (75 mg/kg), and xylazine (5 mg/kg)) and underwent either a 30 min stimulation, sham stimulation (electrodes placed without current delivery), or photothrombosis stroke (PT) as previously described (Lippmann et al., 2017). Briefly, Rose Bengal was administered intravenously (20 mg/kg) and a halogen light beam was directed for 15 min onto the intact exposed skull over the right somatosensory cortex. Then, rats were deeply anaesthetized and transcardially perfused with cold PBS, and brains were extracted at different time points following stimulation (immediately (real and sham), 4 and 24 h post) and 24 h post stroke. The ipsi- and contra lateral somatosensory cortices were dissected, weighed, and snap-frozen on dry ice. Fresh frozen samples were then homogenized in PBS + 1% Triton X-100 (v/v). Tissue homogenates were centrifuged at 13000 g for 10 min and supernatants were stored at -80°C until further analysis. Albumin levels were determined in diluted samples, using the Rat Albumin ELISA kit (Bethyl Laboratories, TX, USA) according to the manufacturer's instructions.

Western Blotting

Brain tissues were collected from stimulated and control rats as described above. Protein lysates were separated using 10% sodium dodecyl sulfate polyacrylamide gel electrophoresis (SDS–PAGE, Bio-Rad) and then transferred to nitrocellulose membranes (Bio-Rad). Membranes were washed with TBS + 0.1% Tween20 (TBST, 3 x 5 min), then blocked with 5% BSA in TBS for 1 h. Membranes were then incubated overnight at 4°C with primary antibodies, followed by 2 h incubation with secondary antibodies. Protein bands were visualized with the enhanced chemiluminescent HRP substrate Crescendo Immobilon (Millipore). Analysis was performed in ImageJ, and band density levels were expressed as fold-changes to controls after normalization to β-actin and controls within the same blot. Primary antibodies used were mouse anti-PSD-95 (1:1500, Thermo Fisher Scientific, MA1-045), anti-β-actin (Loading control, 1:2000, Abcam, ab8226). Secondary antibodies were Goat anti-mouse (1:4000, Abcam, ab205719) and Goat anti-rabbit (1:4000, Abcam, ab97051).

RNA Extraction & Purification

Total RNA was extracted from 100-150 mg of flash-frozen rat somatosensory cortex tissue using TRIzol reagent (ThermoFisher Scientific #15596026) as previously described (Rio et al., 2010). Glycoblue (Invitrogen #AM9515) was added to assist with RNA pellet isolation. Pellets were washed with 75% ethanol and allowed to dry before being dissolved in 20 µL of RNase-DNase free water. 2 µL of 10x DNase I Buffer (New England Biolabs, #m0303s), 1 µL of rDNase I (ThermoFisher Scientific, AM2235), and DNase Inactivation Reagent (ThermoFisher Scientific, AM1907) were added to each RNA sample for purification.

RNA Sequencing & Bioinformatics

Library preparation was performed by the QB3-Berkeley Functional Genomics Laboratory at UC Berkeley. mRNA selection was done with the oligo-dT beads. Both total RNA and oligo dT bead selected mRNA quality was assessed on an Agilent 2100 Bioanalyzer. Libraries were prepared using the KAPA RNA Hyper Prep kit (Roche KK8540). Truncated universal stub adapters were ligated to cDNA fragments, which were then extended via PCR using unique dual indexing primers into full length Illumina adapters. Library quality was checked on an AATI (now Agilent) Fragment Analyzer. Libraries were then transferred to the QB3-Berkeley Vincent J. Coates Genomics Sequencing Laboratory, also at UC Berkeley. Library molarity was measured via quantitative PCR with the KAPA Library Quantification Kit (Roche KK4824) on a BioRad CFX Connect thermal cycler. Libraries were then pooled by molarity and sequenced on an Illumina NovaSeq 6000 S4 flowcell for 2 x 150 cycles, targeting at least 25M reads per sample. Fastq files were generated and demultiplexed using Illumina bcl2fastq2 v2.20. No other processing, trimming, or filtering was conducted. RNA-seq reads were aligned using STAR v2.9.1a against UCSC rat genome rn6. Downstream analysis was performed using FastQC v0.11.9, MultiQC v1.11, and featureCounts. R studio was used for data analysis, R v4.0.2. with the packages tidyverse v1.3.1, IHW, DESeq2. Gene ontology (GO) analysis of enriched genes in ipsi- and contra-lateral somatosensory cortices of stimulated rats was performed using Metascape (Zhou et al., 2019) (http://metascape.org/). Analysis of cell-specific and vascular zonation genes was performed as described (Vanlandewijck et al., 2018), using the database provided in (http://betsholtzlab.org/VascularSingleCells/database.html).

Magnetic Resonance Imaging

Participants

All procedures were approved by the Soroka University Medical Center Institutional Review Board. All participants gave their written informed consent before participation.

Six healthy adult individuals (18-35 years of age) were recruited to perform a motor task while undergoing MRI. Data from 10 age-matched control subjects that did not perform the task were also analyzed.

Data acquisition

MRI scans were performed in the imaging center at the Soroka Medical Center using a 3T Philips Ingenia MRI scanner. A high-resolution T1-weighted anatomical scan (3D gradient echo, TE/TR 3.7/8.2 ms, voxel size of 1 mm^3, 256 x 256 acquisition matrix), followed by a T2-weighted scan (TE/TR = 90/3000 ms, voxel size 0.45 x 0.45 x 4 mm). Functional data were collected by using a gradient echo EPI, with voxel size of 3 x 3 x 3 mm, TE/TR = 35/2000 ms, 83 x 80 acquisition matrix, flip angle of 90°, and FOV 109 mm. For calculation of pre-contrast longitudinal relaxation times, variable flip angle method was used (3D T1w-FFE, TE/TR = 2/10 ms, acquisition matrix: 256 x 256, voxel size: 0.89 x 0.89 x 6 mm, flip angles: 5, 15, 20 and 25°). Dynamic contrast-enhanced (DCE) sequence was then acquired (Axial, 3D T1w-FFE, TE/TR = 2/4 ms, acquisition matrix: 192 x 187 (reconstructed to 256 x 256), voxel size: 0.9 x 0.9 x 6 mm, flip angle: 20°, Δt = 10 s, temporal repetitions: 100, total scan length: 16.7 min). An intravenous bolus injection (0.1 mmol/kg, 0.5 M) of the contrast agent gadoterate meglumine (Gd-DOTA, Dotarem, Guerbet, France) was administered using an automatic injector after 5 dynamic scans at a rate of 1.5 ml/s.

Preprocessing of functional data

fMRI data preprocessing was performed using the Statistical Parametric Mapping package (SPM12; Wellcome Trust Centre for Neuroimaging, London, UK) for

MATLAB. The first ten functional images of each run series were discarded to allow stabilization of the magnet. Functional images were realigned and co-registered to the T1-weighted structural image, followed by segmentation and normalization to the Montreal Neurological Institute (MNI) space. Spatial smoothing using Gaussian kernel (FWHM of 6 mm) was performed.

fMRI Localizer Motor Task

For the motor localizer task, participants were provided with an elastic hand-ball (stress ball), and were asked to press continuously with their strong hand on the Go cue (green screen) and stop on the Stop cue (red screen) for a total of 4 experimental blocks. Both the beginning and the end of the motor localizer task consisted of a fixation block. Task-related activation was evaluated for each contrast, and the voxel values constituted a statistical parametric map of the t-statistic. The statistical threshold for clusters was set at $p<0.05$ and corrected for multiple comparisons using family-wise error (FWE) over the whole brain (uncorrected threshold $p<0.001$) to minimize detection of false positives (type I error).

BBB permeability quantification

Analysis was performed as reported (Serlin et al., 2019; Veksler et al., 2020). Briefly, preprocessing included image registration and normalization to MNI space using SPM12. BBB permeability was calculated using in-house MATLAB script. A linear fit was applied to the later stage of the scan and the slope of contrast agent concentration changes over time was calculated for each voxel. Positive slopes reflected contrast agent accumulation due to BBB modulation. To compensate for physiological (e.g., heart rate, blood flow) and technical (e.g., injection rate) variability, slopes were normalized to the slope of each subject's transverse sinus. Values were considered to reflect modulated BBB when exceeding the 95th percentile of the corresponding mean

cumulative distribution function from healthy young controls. Voxels that reflect modulated BBB values were color-coded and superimposed on the anatomical scans to illustrate the kinetics, localization, and extent of BBB pathology.

Statistical analysis

All statistical tests were performed using Prism9 (GraphPad Software) and are indicated in the figure legends. Tests were two-tailed and corrected for multiple comparisons with two-stage linear step-up false discovery rate (FDR) procedure of Benjamini, Krieger and Yekutieli whenever applicable. Paired tests were used for inter-hemispheric comparisons. Non-parametric tests were used for data which was not normally distributed. $P \leq 0.05$ was defined as the statistical significance level.

Data and Code Availability

Source Data for quantification described in the text or shown in Figs. 1–4 and Extended Data Figure 1–4 are available with the paper. Additional data are available upon reasonable requests. Code and custom MATLAB scripts for analyses used in this study is also available upon reasonable request from the corresponding authors.

References

Andreone, B.J., Chow, B.W., Tata, A., Lacoste, B., Ben-Zvi, A., Bullock, K., Deik, A.A., Ginty, D.D., Clish, C.B., and Gu, C. (2017). Blood-brain barrier permeability is regulated by lipid transport-dependent suppression of caveolae-mediated transcytosis. Neuron *94*, 581. https://doi.org/10.1016/J.NEURON.2017.03.043.

Bouchard, M.B., Chen, B.R., Burgess, S.A., and Hillman, E.M.C. (2009). Ultra-fast multispectral optical imaging of cortical oxygenation, blood flow, and intracellular calcium dynamics. Opt. Express *17*, 15670. https://doi.org/10.1364/oe.17.015670.

Cacheaux, L.P., Ivens, S., David, Y., Lakhter, A.J., Bar-Klein, G., Shapira, M., Heinemann, U., Friedman, A., and Kaufer, D. (2009). Transcriptome profiling reveals TGF-β signaling involvement in epileptogenesis. J. Neurosci. *29*, 8927–8935. https://doi.org/10.1523/JNEUROSCI.0430-09.2009.

Chow, B.W., and Gu, C. (2015). The Molecular Constituents of the Blood-Brain

Barrier. Trends Neurosci. *38*, 598–608. https://doi.org/10.1016/j.tins.2015.08.003.

Chow, B.W., Nuñez, V., Kaplan, L., Granger, A.J., Bistrong, K., Zucker, H.L., Kumar, P., Sabatini, B.L., and Gu, C. (2020). Caveolae in CNS arterioles mediate neurovascular coupling. Nature *579*, 106–110. https://doi.org/10.1038/s41586-020-2026-1.

Classen, J., Liepert, J., Wise, S.P., Hallett, M., and Cohen, L.G. (1998). Rapid plasticity of human cortical movement representation induced by practice. J. Neurophysiol. *79*, 1117–1123. https://doi.org/10.1152/JN.1998.79.2.1117/ASSET/IMAGES/LARGE/JNP.JA47F4.JPEG.

Dahlmanns, M., Dahlmanns, J.K., Schmidt, C.C., Valero-Aracama, M.J., Zheng, F., and Alzheimer, C. (2022). Environmental enrichment recruits activin A to recalibrate neural activity in mouse hippocampus. Cereb. Cortex https://doi.org/10.1093/cercor/bhac092.

David, Y., Cacheaux, L.P., Ivens, S., Lapilover, E., Heinemann, U., Kaufer, D., and Friedman, A. (2009). Astrocytic dysfunction in epileptogenesis: Consequence of altered potassium and glutamate homeostasis? J. Neurosci. *29*, 10588–10599. https://doi.org/10.1523/JNEUROSCI.2323-09.2009.

Draganski, B., Gaser, C., Busch, V., Schuierer, G., Bogdahn, U., and May, A. (2004). Changes in grey matter induced by training. Nature *427*, 311–312. https://doi.org/10.1038/427311a.

El-Husseini, A.E., Schnell, E., Chetkovich, D.M., Nicoll, R.A., and Bredt, D.S. (2000). PSD-95 involvement in maturation of excitatory synapses. Science (80-.). *290*, 1364–1368. https://doi.org/10.1126/science.290.5495.1364.

Gradari, S., Herrera, A., Tezanos, P., Fontán-Lozano, Á., Pons, S., and Trejo, J.L. (2021). The role of Smad2 in adult neuroplasticity as seen through hippocampal-dependent spatial learning/memory and neurogenesis. J. Neurosci. *41*, 6836–6849. https://doi.org/10.1523/JNEUROSCI.2619-20.2021.

Halder, P., Sterr, A., Brem, S., Bucher, K., Kollias, S., and Brandeis, D. (2005). Electrophysiological evidence for cortical plasticity with movement repetition. Eur. J. Neurosci. *21*, 2271–2277. https://doi.org/10.1111/J.1460-9568.2005.04045.X.

Hawkins, B.T., Ocheltree, S.M., Norwood, K.M., and Egleton, R.D. (2007). Decreased blood–brain barrier permeability to fluorescein in streptozotocin-treated rats. Neurosci. Lett. *411*, 1–5. https://doi.org/10.1016/J.NEULET.2006.09.010.

Heinemann, U., Kaufer, D., and Friedman, A. (2012). Blood-brain barrier dysfunction, TGFβ signaling, and astrocyte dysfunction in epilepsy. Glia *60*, 1251–1257. https://doi.org/10.1002/glia.22311.

Hillman, C.H., Erickson, K.I., and Kramer, A.F. (2008). Be smart, exercise your heart: Exercise effects on brain and cognition. Nat. Rev. Neurosci. *9*, 58–65. https://doi.org/10.1038/nrn2298.

Holtmaat, A., and Svoboda, K. (2009). Experience-dependent structural synaptic plasticity in the mammalian brain. Nat. Rev. Neurosci. *10*, 647–658. https://doi.org/10.1038/nrn2699.

Ivens, S., Kaufer, D., Flores, L.P., Bechmann, I., Zumsteg, D., Tomkins, O., Seiffert,

E., Heinemann, U., and Friedman, A. (2007). TGF-β receptor-mediated albumin uptake into astrocytes is involved in neocortical epileptogenesis. Brain *130*, 535–547. https://doi.org/10.1093/brain/awl317.

John, T.A., Vogel, S.M., Tiruppathi, C., Malik, A.B., and Minshall, R.D. (2003). Quantitative analysis of albumin uptake and transport in the rat microvessel endothelial monolayer. Am. J. Physiol. - Lung Cell. Mol. Physiol. *284*, L187–L196. https://doi.org/10.1152/ajplung.00152.2002.

Kim, S.Y., Senatorov, V. V., Morrissey, C.S., Lippmann, K., Vazquez, O., Milikovsky, D.Z., Gu, F., Parada, I., Prince, D.A., Becker, A.J., et al. (2017). TGFβ signaling is associated with changes in inflammatory gene expression and perineuronal net degradation around inhibitory neurons following various neurological insults. Sci. Rep. *7*, 7711. https://doi.org/10.1038/s41598-017-07394-3.

Kleim, J.A., Cooper, N.R., and VandenBerg, P.M. (2002). Exercise induces angiogenesis but does not alter movement representations within rat motor cortex. Brain Res. *934*, 1–6. https://doi.org/10.1016/S0006-8993(02)02239-4.

Levi, H., Schoknecht, K., Prager, O., Chassidim, Y., Weissberg, I., Serlin, Y., and Friedman, A. (2012). Stimulation of the Sphenopalatine Ganglion Induces Reperfusion and Blood-Brain Barrier Protection in the Photothrombotic Stroke Model. PLoS One *7*, e39636. https://doi.org/10.1371/journal.pone.0039636.

Lippmann, K., Kamintsky, L., Kim, S.Y., Lublinsky, S., Prager, O., Nichtweiss, J.F., Salar, S., Kaufer, D., Heinemann, U., and Friedman, A. (2017). Epileptiform activity and spreading depolarization in the blood-brain barrier-disrupted peri-infarct hippocampus are associated with impaired GABAergic inhibition and synaptic plasticity. J. Cereb. Blood Flow Metab. *37*, 1803–1819. https://doi.org/10.1177/0271678X16652631.

McMillin, M.A., Frampton, G.A., Seiwell, A.P., Patel, N.S., Jacobs, A.N., and DeMorrow, S. (2015). TGFβ1 exacerbates blood-brain barrier permeability in a mouse model of hepatic encephalopathy via upregulation of MMP9 and downregulation of claudin-5. Lab. Investig. *95*, 903–913. https://doi.org/10.1038/labinvest.2015.70.

Nishijima, T., Piriz, J., Duflot, S., Fernandez, A.M., Gaitan, G., Gomez-Pinedo, U., Verdugo, J.M.G., Leroy, F., Soya, H., Nuñez, A., et al. (2010). Neuronal Activity Drives Localized Blood-Brain-Barrier Transport of Serum Insulin-like Growth Factor-I into the CNS. Neuron *67*, 834–846. https://doi.org/10.1016/j.neuron.2010.08.007.

Pan, W., and Kastin, A.J. (2017). The blood-brain barrier: Regulatory roles in wakefulness and sleep. Neuroscientist *23*, 124–136. https://doi.org/10.1177/1073858416639005.

Patel, M.R., and Weaver, A.M. (2021). Astrocyte-derived small extracellular vesicles promote synapse formation via fibulin-2-mediated TGF-β signaling. Cell Rep. *34*, 108829. https://doi.org/10.1016/J.CELREP.2021.108829/ATTACHMENT/94D8743E-DD63-4C6F-A978-342014ADF700/MMC2.XLSX.

Prager, O., Chassidim, Y., Klein, C., Levi, H., Shelef, I., and Friedman, A. (2010). Dynamic in vivo imaging of cerebral blood flow and blood-brain barrier permeability. Neuroimage *49*, 337–344. https://doi.org/10.1016/j.neuroimage.2009.08.009.

Pulido, R.S., Munji, R.N., Chan, T.C., Quirk, C.R., Weiner, G.A., Weger, B.D., Rossi, M.J., Elmsaouri, S., Malfavon, M., Deng, A., et al. (2020). Neuronal Activity Regulates Blood-Brain Barrier Efflux Transport through Endothelial Circadian Genes. Neuron *108*, 937-952.e7. https://doi.org/10.1016/j.neuron.2020.09.002.

Revah, O., Lasser-Katz, E., Fleidervish, I.A., and Gutnick, M.J. (2016). The earliest neuronal responses to hypoxia in the neocortical circuit are glutamate-dependent. Neurobiol. Dis. *95*, 158–167. https://doi.org/10.1016/J.NBD.2016.07.019.

Rio, D.C., Ares, M., Hannon, G.J., and Nilsen, T.W. (2010). Purification of RNA using TRIzol (TRI Reagent). Cold Spring Harb. Protoc. *5*, pdb.prot5439. https://doi.org/10.1101/pdb.prot5439.

Sagi, Y., Tavor, I., Hofstetter, S., Tzur-Moryosef, S., Blumenfeld-Katzir, T., and Assaf, Y. (2012). Learning in the Fast Lane: New Insights into Neuroplasticity. Neuron *73*, 1195–1203. https://doi.org/10.1016/j.neuron.2012.01.025.

Saunders, N.R., Dziegielewska, K.M., Møllgård, K., and Habgood, M.D. (2015). Markers for blood-brain barrier integrity: How appropriate is Evans blue in the twenty-first century and what are the alternatives? Front. Neurosci. *9*, 385. https://doi.org/10.3389/fnins.2015.00385.

Schnitzer, J.E., and Oh, P. (1994). Albondin-mediated capillary permeability to albumin. Differential role of receptors in endothelial transcytosis and endocytosis of native and modified albumins. J. Biol. Chem. *269*, 6072–6082. https://doi.org/10.1016/s0021-9258(17)37571-3.

Schoknecht, K., Prager, O., Vazana, U., Kamintsky, L., Harhausen, D., Zille, M., Figge, L., Chassidim, Y., Schellenberger, E., Kovács, R., et al. (2014). Monitoring stroke progression: In vivo imaging of cortical perfusion, blood-brain barrier permeability and cellular damage in the rat photothrombosis model. J. Cereb. Blood Flow Metab. *34*, 1791–1801. https://doi.org/10.1038/jcbfm.2014.147.

Seiffert, E., Dreier, J.P., Ivens, S., Bechmann, I., Tomkins, O., Heinemann, U., and Friedman, A. (2004). Lasting blood-brain barrier disruption induces epileptic focus in the rat somatosensory cortex. J. Neurosci. *24*, 7829–7836. https://doi.org/10.1523/JNEUROSCI.1751-04.2004.

Serlin, Y., Ofer, J., Ben-Arie, G., Veksler, R., Ifergane, G., Shelef, I., Minuk, J., Horev, A., and Friedman, A. (2019). Blood-Brain Barrier Leakage: A New Biomarker in Transient Ischemic Attacks. Stroke *50*, 1266–1269. https://doi.org/10.1161/STROKEAHA.119.025247.

Skotland, T., Kavaliauskiene, S., and Sandvig, K. (2020). The role of lipid species in membranes and cancer-related changes. Cancer Metastasis Rev. *39*, 343–360. https://doi.org/10.1007/s10555-020-09872-z.

Tiruppathi, C., Song, W., Bergenfeldt, M., Sass, P., and Malik, A.B. (1997). Gp60 Activation Mediates Albumin Transcytosis in Endothelial Cells by Tyrosine Kinase-dependent Pathway. J. Biol. Chem. *272*, 25968–25975. https://doi.org/10.1074/JBC.272.41.25968.

Vanlandewijck, M., He, L., Mäe, M.A., Andrae, J., Ando, K., Del Gaudio, F., Nahar, K., Lebouvier, T., Laviña, B., Gouveia, L., et al. (2018). A molecular atlas of cell types and zonation in the brain vasculature. Nature *554*, 475–480. https://doi.org/10.1038/nature25739.

Vazana, U., Veksler, R., Pell, G.S., Prager, O., Fassler, M., Chassidim, Y., Roth, Y., Shahar, H., Zangen, A., Raccah, R., et al. (2016). Glutamate-mediated blood–brain barrier opening: Implications for neuroprotection and drug delivery. J. Neurosci. *36*, 7727–7739. https://doi.org/10.1523/JNEUROSCI.0587-16.2016.

Veksler, R., Vazana, U., Serlin, Y., Prager, O., Ofer, J., Shemen, N., Fisher, A.M., Minaeva, O., Hua, N., Saar-Ashkenazy, R., et al. (2020). Slow blood-to-brain transport underlies enduring barrier dysfunction in American football players. Brain *143*, 1826–1842. https://doi.org/10.1093/brain/awaa140.

Weissberg, I., Wood, L., Kamintsky, L., Vazquez, O., Milikovsky, D.Z., Alexander, A., Oppenheim, H., Ardizzone, C., Becker, A., Frigerio, F., et al. (2015). Albumin induces excitatory synaptogenesis through astrocytic TGF-β/ALK5 signaling in a model of acquired epilepsy following blood-brain barrier dysfunction. Neurobiol. Dis. *78*, 115–125. https://doi.org/10.1016/j.nbd.2015.02.029.

Yang, A.C., Stevens, M.Y., Chen, M.B., Lee, D.P., Stähli, D., Gate, D., Contrepois, K., Chen, W., Iram, T., Zhang, L., et al. (2020). Physiological blood–brain transport is impaired with age by a shift in transcytosis. Nature *583*, 425–430. https://doi.org/10.1038/s41586-020-2453-z.

Zhang, S.L., Yue, Z., Arnold, D.M., Artiushin, G., and Sehgal, A. (2018). A Circadian Clock in the Blood-Brain Barrier Regulates Xenobiotic Efflux. Cell *173*, 130-139.e10. https://doi.org/10.1016/j.cell.2018.02.017.

Zhou, Y., Zhou, B., Pache, L., Chang, M., Khodabakhshi, A.H., Tanaseichuk, O., Benner, C., and Chanda, S.K. (2019). Metascape provides a biologist-oriented resource for the analysis of systems-level datasets. Nat. Commun. *10*, 1–10. https://doi.org/10.1038/s41467-019-09234-6.